

Optimization of the optical and electrical properties of electron beam evaporated aluminum-doped zinc oxide films for opto-electronic applications

H.M. Ali*, M.M. Abd El-Raheem, N.M. Megahed, H.A. Mohamed

Physics Department, Faculty of Science, South Valley University, 82524 Sohag, Egypt

Received 29 November 2005; received in revised form 11 April 2006; accepted 14 April 2006

Abstract

Aluminum-doped zinc oxide (AZO) thin films have been deposited by electron beam evaporation technique on glass substrates. The structural, electrical and optical properties of AZO films have been investigated as a function of annealing temperature. It was observed that the optical properties such as transmittance, reflectance, optical band gap and refractive index of AZO films were strongly affected by annealing temperature. The transmittance values of 84% in the visible region and 97% in the NIR region were obtained for AZO film annealed at 475 °C. The room temperature electrical resistivity of $4.6 \times 10^{-3} \Omega \text{cm}$ has been obtained at the same temperature of annealing. It was found that the calculated refractive index has been affected by the packing density of the thin films, whereas, the high annealing temperature gave rise to improve the homogeneity of the films. The single-oscillator model was used to analyze the optical parameters such as the oscillator and dispersion energies.

© 2006 Elsevier Ltd. All rights reserved.

Keywords: D. Optical properties of specific thin films; D. Electrical properties of specific thin films

1. Introduction

Transparent conducting oxides (TCOs) have a wide range of applications in a variety of opto-electronic devices. Most TCOs are based on SnO_2 , In_2O_3 , zinc oxide (ZnO) and their mixed compounds are deposited by different physical and chemical techniques. Recently, zinc oxide or impurity-doped zinc oxide films have been actively investigated as alternate materials to ITO because zinc oxide is a nontoxic, inexpensive and abundant material [1].

ZnO is a II–VI n-type semiconductor with an optical band gap of approximately 3.2 eV at room temperature [2]. Its band structure and optical properties are very similar to those of GaN, which is known to be a good material for the fabrication of optical devices such as light-emitting diodes (LED) or laser diodes (LD) [3]. Pure ZnO is an unstable material due to the adsorption of atmospheric oxygen, which decreases the conductivity and modifies its surface

morphology [4]. To stabilize the material against such changes, doping is necessary and this purpose was achieved by adding several dopants of group III elements such as indium [2], boron [5], aluminum [4,6], etc. and with group VII element like fluorine [7]. Aluminum-doped zinc oxide (AZO) films are also wide band gap semiconductors ($E_g = 3.3\text{--}3.9 \text{ eV}$), which show optical transmission in the visible and near-infrared (IR) regions. These unique properties have been widely studied for various practical applications such as solar cells [8] and flat panel display electrodes [9]. They also find applications as surface acoustic devices [10], optical waveguides [11], gas sensors [12] and micro-machined actuators [13]. The physical properties of the films depend strongly on the deposition method, the growth conditions and post deposition treatment. ZnO films have been prepared by several techniques such as sputtering [14], spray pyrolysis [15], pulsed laser ablation [16], reactive evaporation [17], chemical vapor deposition [18], solution growth techniques [19], sol–gel process [20,21] and filtered cathodic vacuum arc technique [3]. To our knowledge, none of the reports

*Corresponding author. Tel.: +20125717062.

E-mail address: hazem95@yahoo.com (H.M. Ali).

mentioned the growth by electron beam evaporation technique, which provides economical and efficient usage of evaporant [22].

The unique combination of electro-optical properties of TCOs, namely a simultaneous occurrence of high visible transparency and high electrical conductivity can be controlled through the material parameters like dielectric constant ϵ' , carrier concentration N and mobility μ [23–25]. TCOs with high carrier mobility are desired for many applications either simply to reduce the sheet resistance or to avoid free carrier absorption in the near infrared range.

In this work, the effect of annealing treatment on the structure, electrical and optical properties of AZO thin films prepared by electron beam evaporation technique has been investigated.

2. Experimental Details

Appropriate portions of highly pure (5 N) ZnO powder and Al slices were used. ZnO was prepared in tablet form using cold pressing technique. Thin films from the prepared tablet and slices were deposited using Edwards high vacuum coating unit model E306A as three layers, where Al is sandwiched between two layers of ZnO under pressure of 6×10^{-6} and 2×10^{-5} Torr before and during film deposition, respectively. The content of Al (in atomic weight) were taken so that the ratio Al/Zn = 0.2. The film thickness (100 ± 15 nm) and the deposition rate (~ 10 nm/min) for ZnO and (~ 5 nm/min) for Al were controlled by means of a digital film thickness monitor model TM200 Maxtek. The substrate temperature during deposition was maintained at 100°C . As-deposited ZnO:Al films have been annealed in air at different temperatures in the range from 200 to 475°C . Investigations of the microstructure were carried out using a Philips - PW1710 X-ray diffractometer with Cu- K_α as a target and Ni as a filter.

The optical transmittance (T) and reflectivity (R) of AZO films have been measured by means of a computer-programmable Jasco V-570 (Japan) double beam spectrophotometer in the wavelength range from 200 to 2500 nm at normal incidence. In the case of reflectivity measurement, an additional attachment model ISN-470 is provided. The spectral dependencies of refractive index, n , optical dielectric constant, ϵ' , and single oscillator parameters (single oscillator energy, E_o , dispersion energy, E_d) were estimated from the optical data. The resistivity measurements were carried out using two-terminal configuration by applying constant voltage to the sample and measuring the current through it using Keithley 614 electrometer. The measurements were achieved at room temperature. Electrical contacts were made by applying silver paste over the surface of the films with separation of 2 mm.

3. Results and Discussion

Fig. 1a shows the X-ray diffraction patterns of the ZnO:Al films for as-deposited and annealed films at

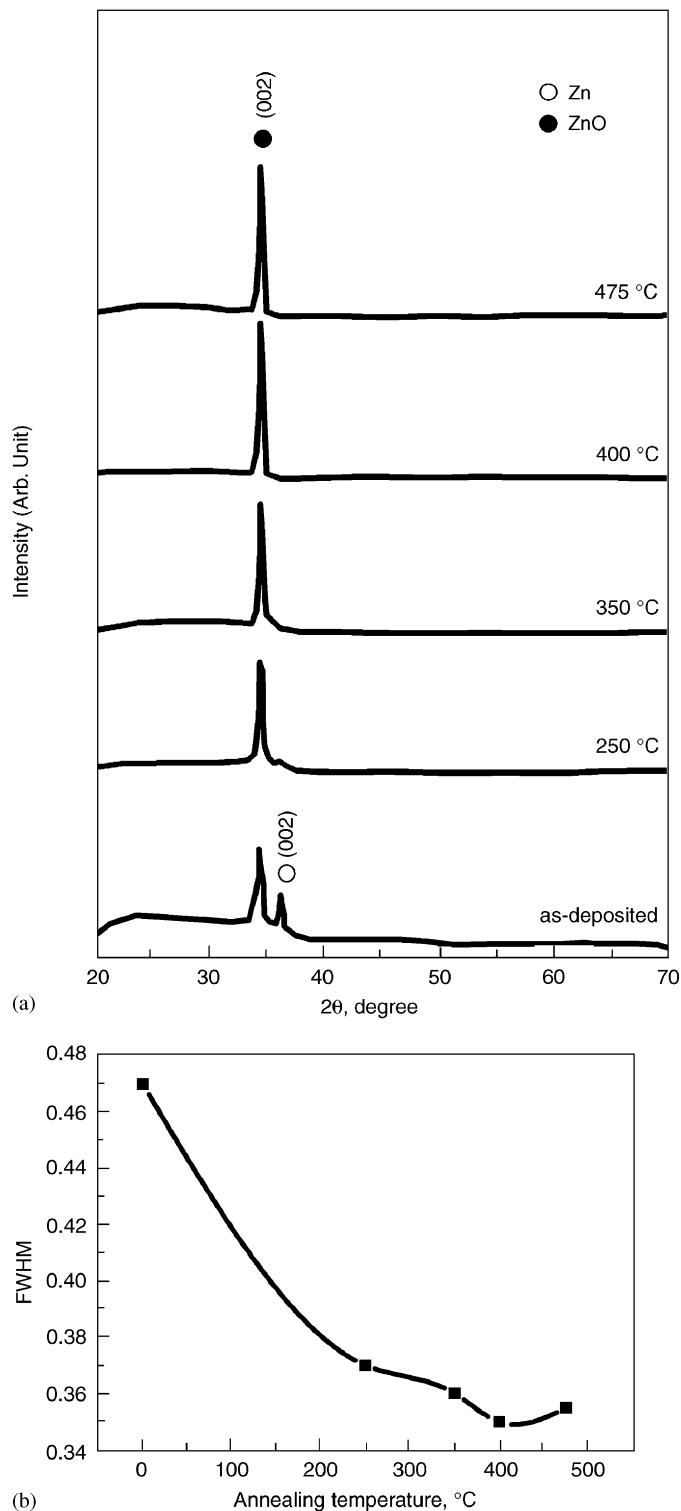


Fig. 1. XRD patterns of AZO thin film annealed at different temperatures (a), and the variation of the FWHM of the (002) ZnO peak with annealing temperature (b).

different annealing temperatures (0, 250, 350, 400 and 475°C). All films are found to have hexagonal wurtzite structure [14]. A prominent (002) ZnO peak located at $2\theta = 34.4^\circ$ indicates that the crystallite structure of the films is oriented with their c -axis perpendicular to the

substrate plane. This value is very close to that of the standard ZnO crystal (34.422°) (JCPDS Card No. 36-1451). For as-deposited film, the appearance of (002) Zn diffraction peak refer to a larger number of oxygen atom vacancies. Upon annealing at 250°C , all atoms of Zn-oxidized and Zn-diffraction peak disappeared. In XRD pattern, no peak of aluminum was observed, which implies that aluminum replaces zinc substitutionally in the hexagonal lattice. It is clear also that, the intensity of the (002) ZnO diffraction peak increases with increasing the temperature of annealing. Meanwhile, as seen in Fig. 1b the full-width at half-maximum (FWHM) decreases with increasing the temperature of annealing. Since the FWHM of the (002) diffraction peak is inversely proportional to the grain size of the film [14], so the grain size of ZnO:Al thin films increases with increasing the annealing temperature.

The typical UV–VIS–NIR optical transmittance and reflectance spectra of AZO films annealed at different annealing temperature as a function of wavelength in the range from 300 to 2500 nm are shown in Fig. 2a and b, respectively. It is clear that the transmittance increases and the reflectance decreases with increasing the annealing temperature from 200 to 475°C . In Fig. 2a, the drop-off of the values of transmission belonging to the shorter wavelengths was related to the fundamental absorption by band-to-band transition. Meanwhile, the wavelength of the absorption edge decreased with an increase in temperature of annealing.

From the transmittance data it is possible to infer the optical gaps of the films by plotting $(\alpha h\nu)^2$ vs. $h\nu$ (where α is the absorption coefficient, and $h\nu$ the photon energy) and by extrapolating the straight line portion of this plot to the energy axis. The obtained values have been plotted in Fig. 3. The optical band gap E_g increases with increase in annealing temperature, which can be explained as follows: the unsaturated defects are gradually annealed out producing a larger number of saturated bonds leading to a decreases in the density of localized states and consequently the optical gap increased. As seen in Fig. 4, it could directly combine the function of transmittance and energy band gap. It is clear that the transmittance in the visible region (in which the solar spectrum is maximum) increases with increasing the optical energy band.

The real dielectric constant ϵ' , which results due to the contribution from the free carrier electric susceptibility, can be written by the following relation [22,26]:

$$\epsilon' = n^2 - k^2 = \epsilon_i - \frac{e^2}{4\pi^2 c^2 \epsilon_o} \left(\frac{N}{m^*} \right) \lambda^2$$

where ϵ_i is the infinitely high-frequency dielectric constant or the residual dielectric constant due to the ion core, e is the electronic charge, c is the velocity of light, ϵ_o is the permittivity of free space and N/m^* is the ratio of carrier concentration to the effective mass. According to the free electron Drude model [27], ϵ' should be a linear function of λ^2 . Fig. 5a shows plots of the real dielectric constant ϵ' vs.

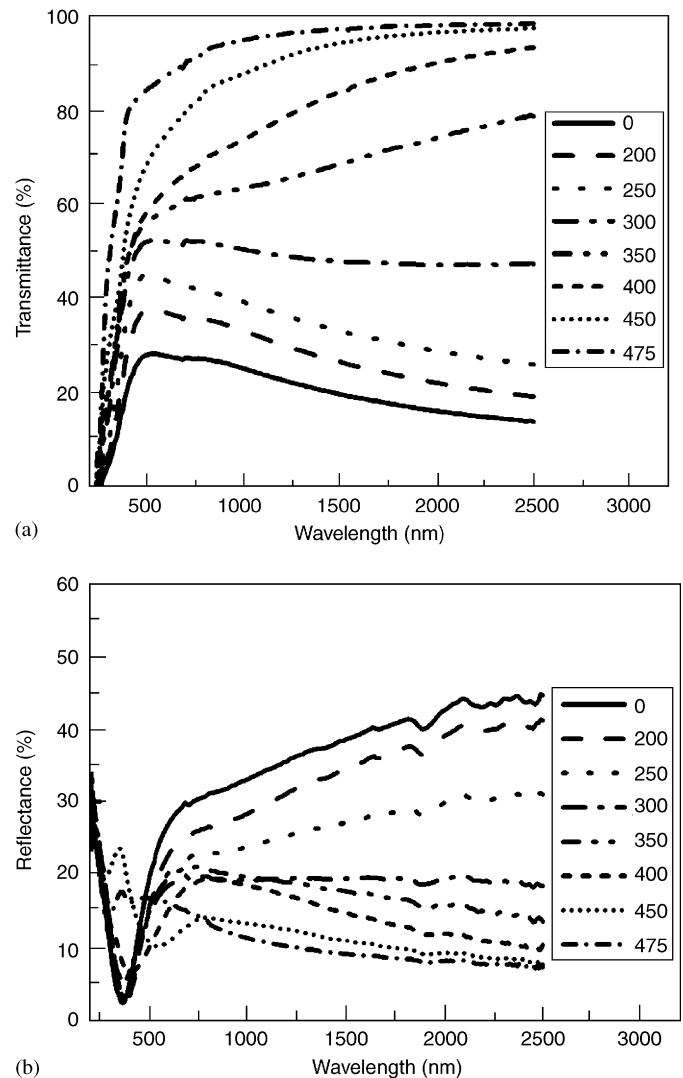


Fig. 2. Optical transmittance (a) and reflectance (b) spectra of AZO film annealed at different temperatures as a function of wavelength.

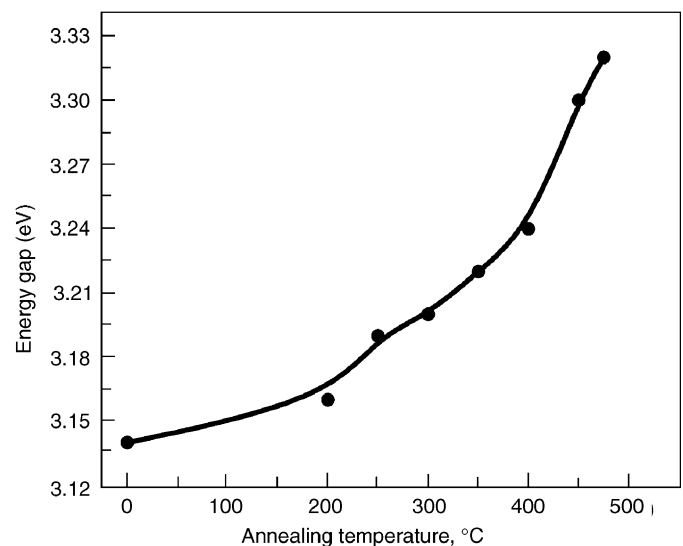


Fig. 3. Annealing temperature dependence of the optical energy gap of AZO thin film.

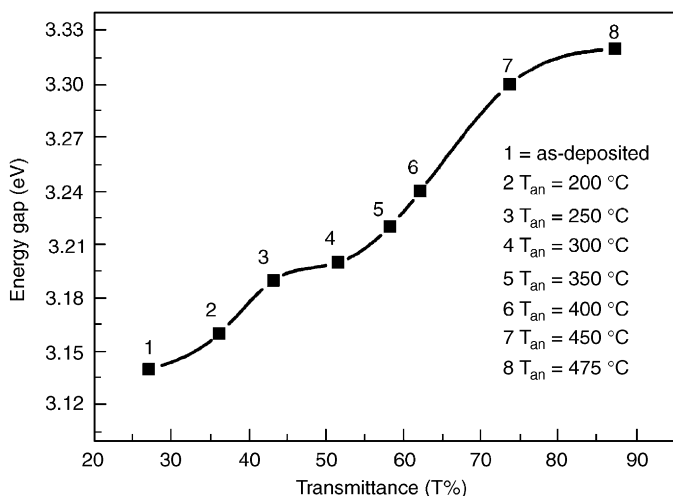
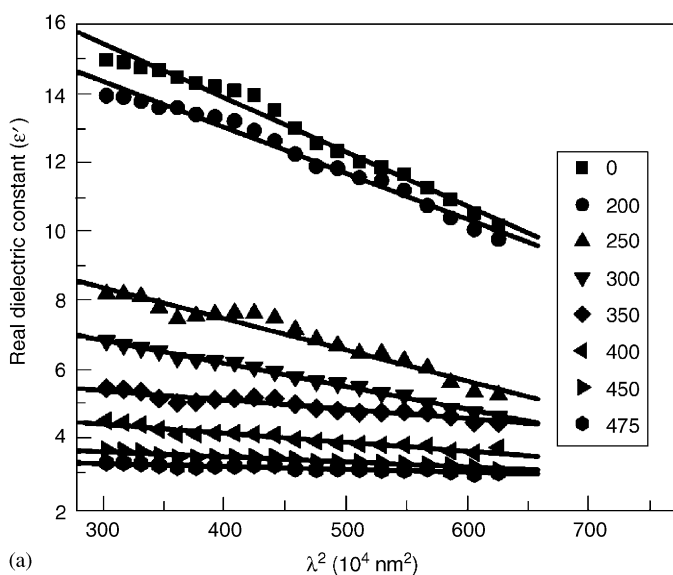
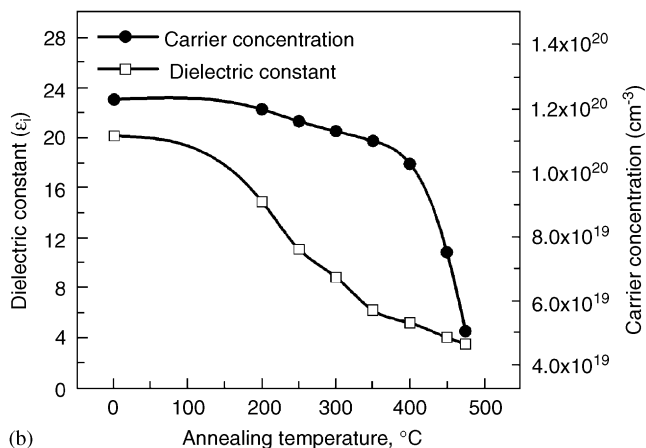


Fig. 4. The average transmittance values of AZO-annealed film in the visible region as a function of energy band gap.



(a)



(b)

Fig. 5. Plots of (a) the real dielectric constant ϵ' vs. the square of wavelength (λ^2); and (b) variations of the residual dielectric constant ϵ_r and free carrier concentration with annealing temperature.

the square of wavelength (λ^2). It can be seen that, the slopes of lines in Fig. 5a decrease with increasing the annealing temperature, this may be due to the decrease of the density of electrons. Values of ϵ_i and N , which were determined from the extrapolations of these plots to $\lambda^2 = 0$ are plotted as a function of annealing conditions as shown Fig 5b. It can be seen that ϵ_i and N decrease with increasing the annealing temperature. In ZnO films, n-type carriers are generated by interstitial Zn atoms acting as donors; thus, a fall in the concentration of interstitial Zn will lead to a fall in carrier concentration. When the films are annealed under ambient air at temperature higher than 400 °C, oxygen is chemisorbed on the film surface and in pores, acting as an acceptor by accepting an electron from occupied conduction band states [28]. Furthermore, the adsorbed oxygen removes zinc interstitials and/or oxygen vacancies, thus reduces the density of donors like defects and carrier concentration [29].

The dependence of electrical properties on the temperature of annealing is shown in Fig. 6. The resistivity initially decreases as the temperature is increased up to 400 °C, after which the resistivity increases with annealing temperature. The lowest resistivity value of $3.2 \times 10^{-3} \Omega \text{ cm}$ has been obtained for annealed film at temperature of 400 °C. It is observable also that, the mobility carriers increased with increase in annealing temperature. This may be due to the increase of the grain size with increase in annealing temperature, and this leads to reduction of the grain boundary scattering due to charge carriers, which consequently increases the mobility of the charge carriers. The decrease of the electrical resistivity of annealed films up to 400 °C is due to the increase of the mobility carriers. For annealed films above 400 °C, the resistivity increases in spite of the increase in the mobility of the charge carriers as the reduction in carrier concentration.

The electronic mean free path L in this study was calculated using the following equation [30]:

$$L = (3\pi^2)^{1/3} (h/e^2) \rho^{-1} N^{-2/3}$$

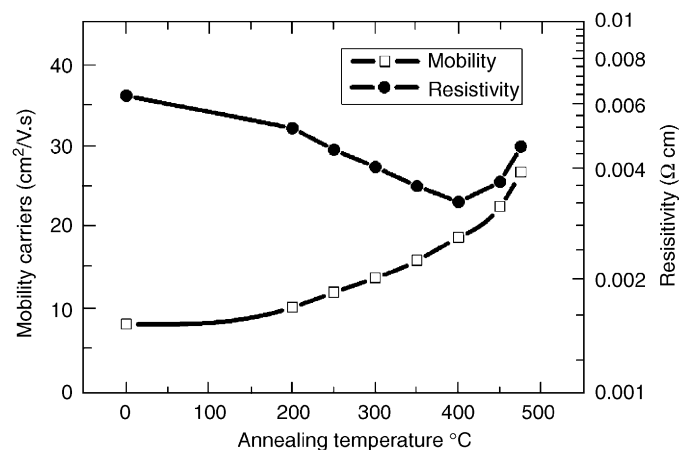


Fig. 6. Variations of the mobility carriers and the room temperature electrical resistivity with annealing temperature.

where h is the Planck's constant, e is the charge on the electron, ρ is the electrical resistivity and N is the free carrier concentration. Fig. 7 depicts the variation of the mean free path of electrons with the annealing temperature of AZO film. The mean free path of electrons increases with increase in temperature of annealing, which can be attributed to the decrease of scattering centers. The variations of refractive index, in the visible wavelength range, of AZO films annealed at different temperatures are shown in Fig. 8a. The extinction coefficient and the average values of the refractive index have been shown in Fig. 8b. The refractive index of the films decreases with increasing the annealing temperature, which can be attributed to the decrease in the packing density with annealing temperature. The packing density of the film can be estimated from the following equation. [31]:

$$n_f^2 = \frac{(1-p)n_v^4 + (1+p)n_v n_s^2}{(1+p)n_v^2 + (1-p)n_s^2},$$

where n_f is the refractive index of AZO film, n_s is the refractive index of the solid part of the film, that for single crystal n_v is the refractive index of the voids (equals one for air), and P is the packing density. The behavior of the backing densities with respect to annealing temperature is shown in Fig. 8b. It has been found that the estimated packing density values decrease with increasing the annealing temperature. It is observable also that the extinction coefficient decreases with increasing the annealing temperature. This could be correlated to the decrease of absorption with increasing the temperature of annealing, where $k = \lambda\alpha/4\pi$, α is the absorption coefficient [32].

Kim [33] reported that, a high percentage of voids exist in the oxide thin films, especially in the surface layer of the thin films. The degree of inhomogeneity of AZO films can be expressed by $(\Delta n/\bar{n}) \%$, where Δn and \bar{n} refer to variation and average values of the refractive index measured at wavelengths in the range of 350–800 nm,

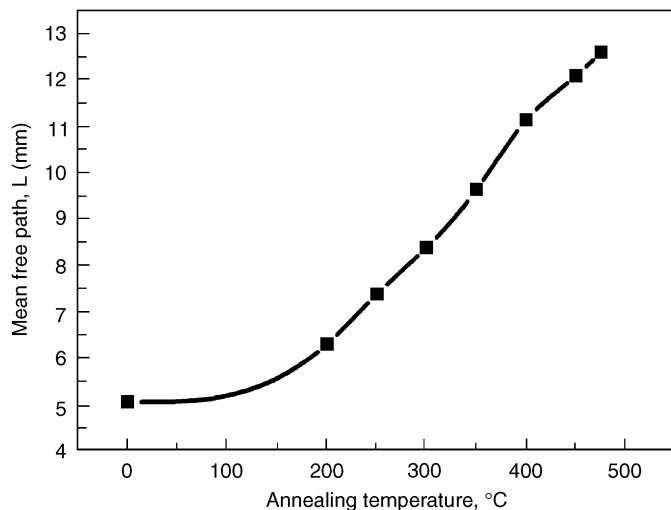
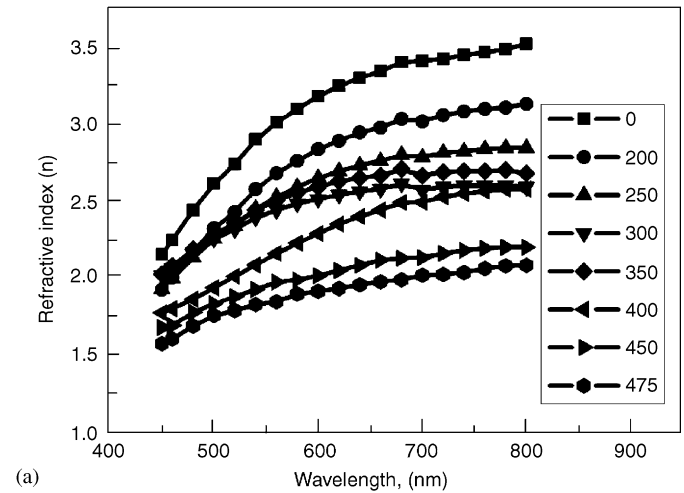
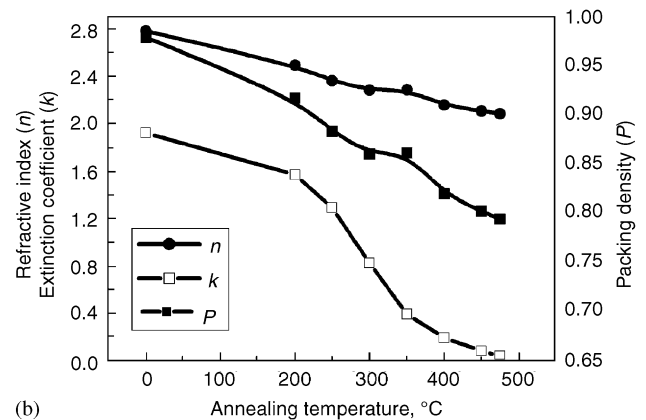


Fig. 7. The mean free path of electrons of AZO thin film as a function of annealing temperatures.

respectively. Fig. 9 shows that a high annealing temperature will give rise to improve the homogeneity of the films, since the degree of inhomogeneity decreased from 7.75% to 3.25%.



(a)



(b)

Fig. 8. Variations of the refractive index with wavelength (a) and the annealing temperature dependence of average refractive index, extinction coefficient in the visible region and the packing density (b) of AZO thin film.

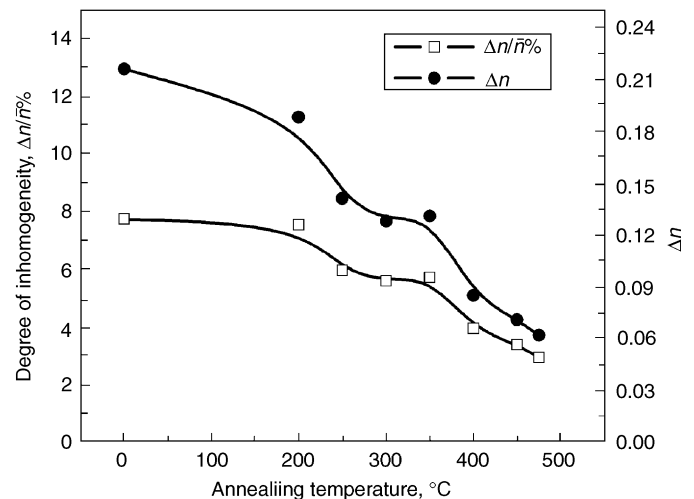


Fig. 9. The degree of inhomogeneity and the variation of the refractive index of AZO film as a function of annealing temperature.

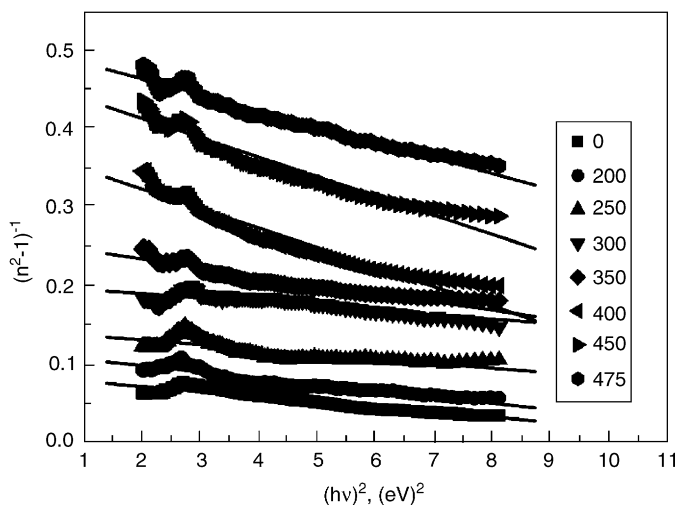


Fig. 10. plots of $(n^2-1)^{-1}$ vs. $(hv)^2$ for AZO annealed film at different temperature.

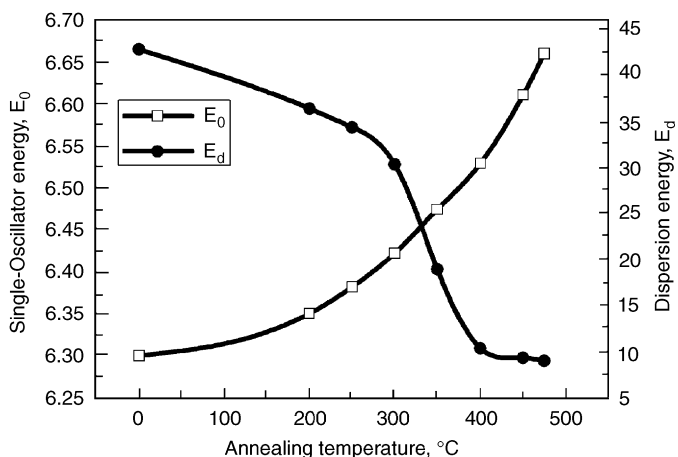


Fig. 11. The variations of E_o and E_d with annealing temperature.

for the as-deposited film to 2.95% for the film annealed at 475 °C. Fig. 9 shows also a smaller variation of the refractive index at elevated temperatures, due to the voids decreasing in the films because of the oxygen vacancies corporation.

The single-oscillator model was used to analyze the optical parameters such as the oscillator and dispersion energies, in which the dispersion of the refractive index is related to the photon energy, $h\nu$, according to the following equation. [32,34]:

$$(n^2 - 1)^{-1} = \frac{E_o}{E_d} - \frac{1}{E_o E_d} (h\nu)^2,$$

where n is the refractive index, h is Planck's constant, ν is the frequency, $h\nu$ is the photon energy, E_o (single oscillator energy) is the average excitation energy for electronic transitions and E_d is the dispersion energy, which is a measure of the strength of interband optical transitions. By plotting $(n^2-1)^{-1}$ vs. $(h\nu)^2$ and fitting a straight line as

shown in Fig. 10, values of E_d and E_o can be determined directly from the slope $(E_d E_o)^{-1}$ and the intercept E_o/E_d on the vertical axis. Fig. 11 depicts the variations of E_o and E_d with annealing temperature. It was observed that the values of E_o increase with increasing the annealing temperature. This may be due to the behavior of the optical energy gap. According to Refs. [32,35], the single oscillator energy E_o is twice the optical energy gap. This is in a good agreement with our results. It is clear also that the dispersion energy E_d has an opposite behavior of E_o .

4. Conclusions

AZO thin films have been deposited by electron beam evaporation technique on glass substrates. The effect of annealing temperature on the structure, electrical and optical properties of AZO thin films was investigated. It was found that all AZO thin films demonstrate *c*-axis preferred orientation with the best crystallinity obtained at 400 °C. The transmittance value of 84% in the visible region and 97% in the NIR region were obtained for AZO film annealed at 475 °C. The room temperature electrical resistivity of $4.6 \times 10^{-3} \Omega \text{cm}$ has been obtained at the same temperature of annealing. The optical energy gap has been found to be equal to 3.32 eV. The mobility carriers and the carrier concentration values were of the order of $26.7 \text{ cm}^2/\text{Vs}$ and $5.1 \times 10^{19} \text{ cm}^{-3}$, respectively. It has found that the calculated refractive index had a relationship with the packing density of the thin films and the high annealing temperature gave rise to improve the homogeneity of the films.

References

- [1] S. Major, S. Kumar, M. Bhatnagar, K.L. Chopra, Appl. Phys. Lett. 49 (1986) 394.
- [2] S.H. Mohamed, H.M. Ali, H.A. Mohamed, A.M. Salem, Eur. Phys. J. Appl. Phys. 31 (2005) 95–99.
- [3] H.W. Lee, S.P. Lau, Y.G. Wang, K.Y. Tse, H.H. Hng, B.K. Tay, J. Cryst. Growth 268 (2004) 596.
- [4] A.E. Jimenez-Gonzalez, J.A.S. Urueta, R. Suarez-Parra, J. Cryst. Growth 192 (1998) 430.
- [5] W.W. Wenas, A. Yamada, M. Konagai, K. Takahashi, Jpn. J. Appl. Phys. 30 (1991) L441.
- [6] T. Tsuchiya, T. Emoto, T. Sei, J. Non-Cryst. Solids 178 (1994) 327.
- [7] M. de la, L. Olvera, A. Maldonado, R. Asomoza, M. Meléndez-Lira, Sol. Energy Mater. Sol. Cells 71 (2002) 61.
- [8] J.A. Anna Selvan, H. Keppner, A. Shah, Mater. Res. Soc. Symp. Proc. 426 (1996) 497.
- [9] M. Ritala, T. Asikainen, M. Leskela, J. Skarp, Mater. Res. Soc. Symp. Proc. 426 (1996) 513.
- [10] V. Gupta, A. Mansingh, J. Appl. Phys. 80 (2) (1996) 1063.
- [11] M. Bertolotti, M.V. Laschena, M. Rossi, A. Ferrari, L.S. Qian, F. Quaranta, A. Valentini, J. Mater. Res. 5 (9) (1990) 1929.
- [12] K.-S. Weibenrieder, J. Müller, Thin Solid Films 300 (1997) 30.
- [13] J.L. Deschanvres, B. Bochu, J.C. Joubert, J. Phys. 4 (3) (1993) 485.
- [14] J. Yoo, J. Lee, S. Kim, K. Yoon, I. Jun Park, S.K. Dhungel, Thin Solid Films 480–481 (2005) 213–217.
- [15] J.-H. Lee, B.-O. Park, Mater. Sci. Eng. B 106 (2004) 242.
- [16] K. Matsubara, P. Fons, K. Iwata, A. Yamada, K. Sakurai, H. Tampo, S. Niki, Thin Solid Films 369 (2003) 431.

- [17] J.-M. Ting, B.S. Tsai, *Mater. Chem. Phys.* 72 (2001) 273.
- [18] C. Zhang, X. Li, J. Bian, W. Yu, X. Gao, *Surf Coat Technol.* 198 (2005) 253.
- [19] A.J. Varkey, A.F. Fort, *Thin Solid Films* 239 (1994) 22.
- [20] R. Maity, S. Kundoo, K.K. Chattopadhyay, *Solar Energy Mater. Solar Cells* 86 (2005) 217–227.
- [21] R.B.H. Tahar, *J. Eur. Ceram. Soc.* 25 (2005) 3301–3306.
- [22] E.K. Shokr, M.M. Wakkad, H.A. Abd El-Ghanny, H.M. Ali, *J. Phys. Chem. of Solids* 61 (2000) 75–85.
- [23] T.J. Coutts, D.L. Young, X. Li, W.P. Mulligan, X. Wu, *J. Vac. Sci. Tech. A* 18 (2000) 2646.
- [24] K.L. Chopra, S. Major, D.K. Pandya, *Thin Solid Films* 102 (1983) 1.
- [25] R. Gordon, *MRS Bull* 25 (2000) 52.
- [26] W.G. Spitzer, H.Y. Fan, *Phys. Rev.* 106 (1957) 882.
- [27] P. Drude, *Z. Phys.* 1 (1900) 161.
- [28] Y.S. Choi, C.G. Lee, S.M. Cho, *Thin Solid Films* 298 (1996) 153.
- [29] H.A. Mohamed, H.M. Ali, S.H. Mohamed, M.M. Abd El-Raheem, *Eur. Phys. J. Appl. Phys.* 34 (2006) 7.
- [30] C. Kittel, *Introduction to Solid State Physics*, seventh ed, Wiley, New York, 1996, pp. 158–159.
- [31] H.A. Macleod, *J. Vac. Sci. Technol. A* 4 (1986) 418.
- [32] A. Abu El-Fadl, G.A. Mohamad, A.B. Abd El-Moiz, M. Rashad, *Physica B* 366 (2005) 44.
- [33] S.Y. Kim, *Appl. Opt.* 35 (1996) 6703.
- [34] H.M. Ali, *Phys. Status Solidi (a)* 202 (14) (2005) 2742.
- [35] K. Tanaka, *Thin Solid Films* 66 (1980) 271.